

1 **Title: Marine biomarkers from ice cores reveal enhanced high-latitude**

2 **Southern Ocean carbon sink during the Antarctic Cold Reversal**

3 **Running head: *Marine biomarkers highlight SO carbon sink***

4 **Authors:** C.J. Fogwill*^{1,2}, C.S.M. Turney^{2,3,4}, L. Menviel⁴, A. Baker², M. E. Weber⁵, B. Ellis⁶,
5 Z.A. Thomas^{2,3,4}, N. R. Golledge^{7,8}, D. Etheridge⁹, M. Rubino^{1,9,10}, D.P. Thornton⁹, T.D. van
6 Ommen^{11,12}, A.D. Moy^{11,12}, M.A.J. Curran^{11,12}, S. Davies¹³, M.I. Bird^{3,14}, N.C. Munksgaard^{14,15},
7 C.M. Rootes¹⁶, H. Millman^{1,4}, J. Vohra², A. Rivera¹⁷, A. Mackintosh¹⁸, J. Pike¹⁹, I.R. Hall¹⁹, E.A.
8 Bagshaw¹⁹, E. Rainsley¹, C. Bronk Ramsey²⁰, M. Montinari¹, A. Cage¹, M. Harris¹, R. Jones^{21†},
9 A. Power²¹, J. Love²¹, J. Young²², L.S. Weyrich^{3,22}, A. Cooper^{3,22}

10 **Affiliations:**

11 ¹School of Geography, Geology and the Environment, University of Keele, Staffordshire, UK

12 ²Palaeontology, Geobiology and Earth Archives Research Centre, School of Biological Earth and
13 Environmental Sciences, University of New South Wales, 2052, Australia

14 ³ARC Centre of Excellence in Australian Biodiversity and Heritage

15 ⁴Climate Change Research Centre, School of Biological Earth and Environmental Sciences,
16 University of New South Wales, 2052, Australia

17 ⁵Steinmann Institute, University of Bonn, Poppelsdorfer Schloss, Bonn, Germany

18 ⁶Research School of Earth Sciences, Australian National University, Canberra, Australia

19 ⁷Antarctic Research Centre, Victoria University of Wellington, Wellington 6140, New Zealand

20 ⁸GNS Science, Lower Hutt, 5001, New Zealand

21 ⁹CSIRO Oceans and Atmosphere, Aspendale, Victoria, 3195 Australia

22 ¹⁰Dipartimento di Matematica e Fisica, Università della Campania "Luigi Vanvitelli", viale
23 Lincoln, 5-81100 Caserta, Italy

24 ¹¹Department of the Environment, Australian Antarctic Division, 203 Channel Highway,
25 Kingston, Tasmania 7050, Australia

26 ¹²Antarctic Climate & Ecosystems Cooperative Research Centre, University of Tasmania,
27 Private Bag 80, Hobart, Tasmania 7001, Australia

28 ¹³Department of Geography, Swansea University, Swansea, United Kingdom

29 ¹⁴Centre for Tropical Environmental and Sustainability Science, College of Science, Technology
30 and Engineering, James Cook University, Cairns, Australia

31 ¹⁵Research Institute for the Environment and Livelihoods, Charles Darwin University, Australia

32 ¹⁶Department of Geography, University of Sheffield, United Kingdom

33 ¹⁷Glaciology and Climate Change Laboratory, Centro de Estudios Científicos, Valdivia, Arturo Prat
34 514, Chile

35 ¹⁸School of Earth, Atmosphere and Environment, Monash University, Melbourne, Australia

36 ¹⁹School of Earth and Ocean Sciences, University of Cardiff, Wales, UK

37 ²⁰Research Laboratory for Archaeology and the History of Art, University of Oxford, Dyson
38 Perrins Building, South Parks Road, Oxford, OX1 3QY, UK

39 ²¹ BioEconomy Centre, The Henry Wellcome building for Biocatalysis, Biosciences, Stocker
40 Road, Exeter University, Exeter, EX4 4QD, UK

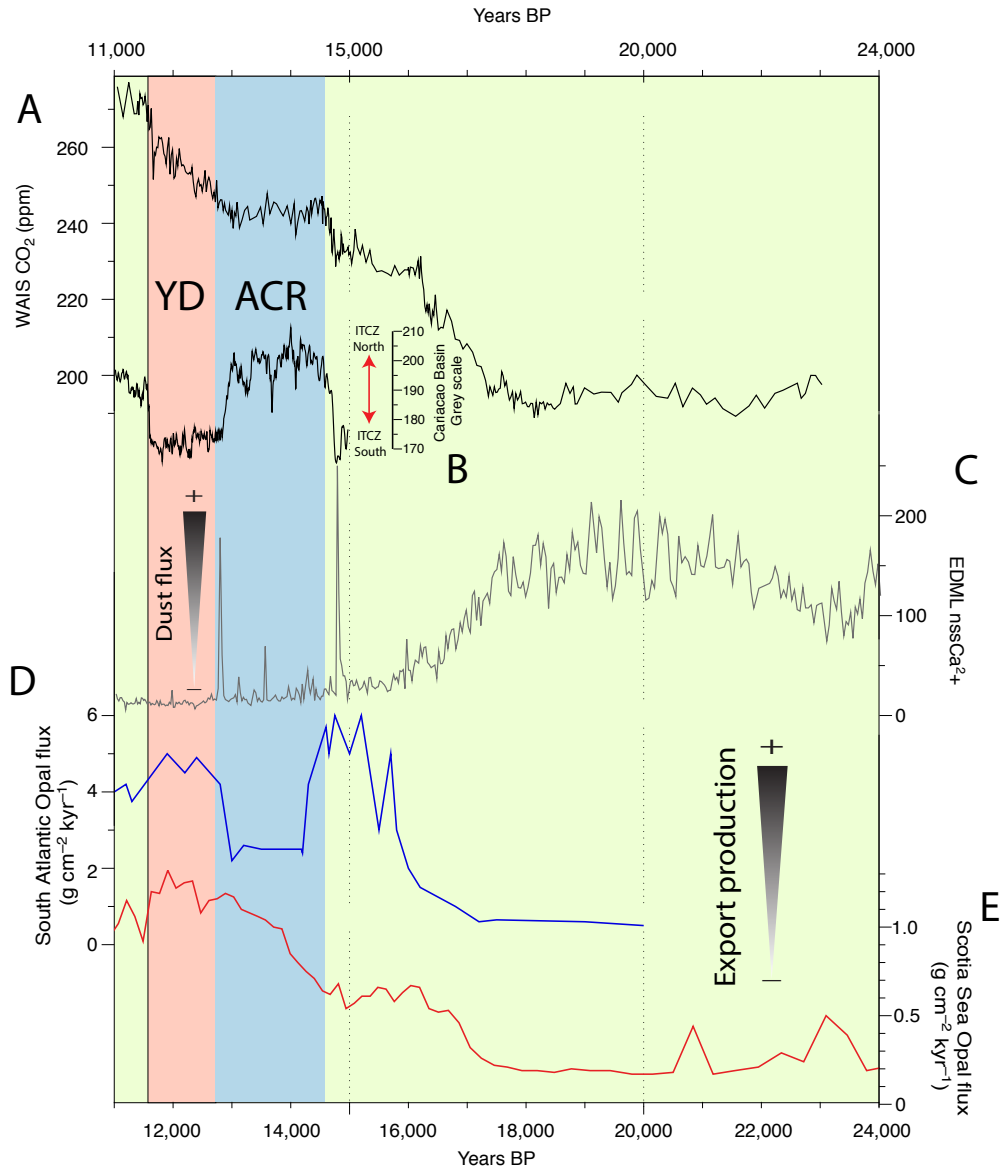
41 ²²Australian Centre for Ancient DNA, University of Adelaide, 5005, Australia

42 Contact Information: *Correspondence to c.j.fogwill@keele.ac.uk

43 **Abstract: The Southern Ocean plays a fundamental role in regulating global atmospheric**
44 **CO₂ levels, yet the underlying processes and feedbacks that control the carbon cycle today**
45 **remain unclear. The Last Glacial Transition (LGT 18,000-11,000 years ago or 18-11 kyr BP)**
46 **experienced rapid and sustained changes in CO₂ that may provide fresh insights, however,**
47 **fundamental questions over the mechanism(s) that modulate climate-carbon dynamics**
48 **during this important period remain. One key example is the enigmatic 1,900-year plateau**
49 **that interrupted the rise in atmospheric CO₂ during the LGT during a period of pronounced**
50 **mid- to high-latitude Southern Hemisphere cooling termed the Antarctic Cold Reversal**
51 **(ACR, 14,600-12,700 years ago or 14.6-12.7 kyr BP). Here we utilise five independent**
52 **approaches to provide a detailed marine biomarker reconstruction from a highly-resolved**
53 **Antarctic ‘horizontal’ ice core. Our reconstruction provides a coherent signal of enhanced**
54 **surface ocean productivity and microbial diversity, in the form of marine picoeukaryotes**
55 **and nanoplankton, that have been captured within ice from precipitation derived from the**
56 **South Atlantic sector of the high-latitude Southern Ocean. When combined with marine**
57 **sediment records, we confirm this period was coincident with increased biological export**
58 **(driving CO₂ sequestration), suggesting high-latitude biological feedbacks contributed to the**
59 **ACR CO₂ plateau. Transient climate modelling indicates that this period coincided with the**
60 **maximum seasonal variability in sea-ice extent, implying sea-ice feedbacks enhanced CO₂**
61 **sequestration, making the high-latitude South Atlantic sector Southern Ocean a significant**
62 **carbon sink that contributed to the sustained plateau in CO₂ levels during the ACR. This**
63 **finding has ramifications for our understanding of contemporary ice-ocean-carbon**
64 **feedbacks, and confirms the dynamic role Antarctic sea ice plays, providing a negative**
65 **feedback during periods of rising CO₂, a result that requires detailed assessment given recent**

66 **high-latitude sea ice changes, that may impact the efficiency of the Southern Ocean carbon**
67 **sink.**

68 **Introduction:** The Southern Ocean occupies some 14% of the planet's surface and plays a
69 fundamental role in the global carbon cycle and climate (Bauska et al., 2016; Le Quéré et al., 2007;
70 Marshall and Speer, 2012). It provides a direct connection to the deep ocean carbon reservoir
71 through physical and biological processes that include surface primary productivity,
72 remineralisation of carbon at depth, and upwelling of carbon-rich and radiocarbon (^{14}C)-depleted
73 water masses (Gottschalk et al., 2016; Marshall and Speer, 2012; Turney et al., 2016). However,
74 the role of these different processes in modulating past and future air-sea carbon flux remains
75 poorly understood (Hewitt et al., 2016; Schmitt et al., 2012). Considerable uncertainty surrounds
76 the source(s) and sink(s) of carbon during the Last Glacial Termination (LGT; 19 to 11.6 kyr BP)
77 when atmospheric CO_2 rose from approximately 190 parts per million (ppm) to around 270 ppm
78 (Figure 1). Recent detailed analysis of the stable isotopic composition of atmospheric carbon
79 dioxide ($\delta^{13}\text{C}-\text{CO}_2$) from Antarctic ice cores provides new insights into the potential effects of
80 terrestrial carbon in defining rapid rises in CO_2 , but highlighted that CO_2 variability across this
81 period may reflect a combination of sources, sinks and feedbacks (Bauska et al., 2016), that may
82 provide valuable insights into the role of the Southern Ocean processes in modulating global CO_2
83 today (Barnes, 2015).



84

85 **Figure 1.** Comparison of A. Atmospheric CO₂ concentration from the WAIS divide core (WD₂₀₁₄
 86 chronology) (Marcott et al., 2014) with available Southern Hemisphere records of B. Cariaco
 87 Basin grey scale, a measure of latitudinal changes in the trade winds associated with the ITCZ
 88 (Hogg et al., 2016). C. non-sea salt Ca²⁺ flux (nssCa²⁺) from EPICA Dronning Maud Land
 89 (EDML) (Wolff et al., 2006a). D. South Atlantic opal flux from core TN057-13 (Anderson et al.,
 90 2009). E. Scotia Sea opal flux from core MD07-3134 (Weber et al., 2014). Vertical boxes indicate
 91 the periods defined by the Antarctic Cold Reversal (ACR) (blue), the Younger Dryas (YD)

92 chronozone (11.7-12.7 kyr BP).

93

94 The parallel changes in Antarctic temperature and atmospheric CO₂ have been interpreted as
95 climate playing a substantial role in the carbon budget of the Southern Ocean (Anderson et al.,
96 2009; Monnin et al., 2001). Several physical and biological mechanisms have been invoked to
97 explain these observations. These include changes in the strength and/or latitudinal migration of
98 the mid-latitude Southern Hemisphere jet stream and prevailing surface westerly air flow that
99 drives Southern Ocean overturning (Anderson et al., 2009; Marshall and Speer, 2012; Toggweiler
100 et al., 2006), variations in iron (dust) fertilization of subantarctic phytoplankton impacting the
101 efficiency of the Southern Ocean biological carbon pump (Jaccard et al., 2016; Jaccard et al., 2013;
102 Martínez-García et al., 2014), Antarctic sea-ice controlling CO₂ exchange (Butterworth and Miller,
103 2016; Delille et al., 2014) and carbon drawdown (Barnes, 2015), as well as the potential impacts
104 of a warming ocean on CO₂ exchange (Bauska et al., 2016). The role of the Southern Ocean as a
105 source or sink of atmospheric carbon during the LGT remains highly contested, with the above
106 processes not fully accounting for the pattern of change in CO₂ recorded over this period (Jaccard
107 et al., 2016), implying that one or more mechanisms are currently not captured in our present
108 understanding.

109

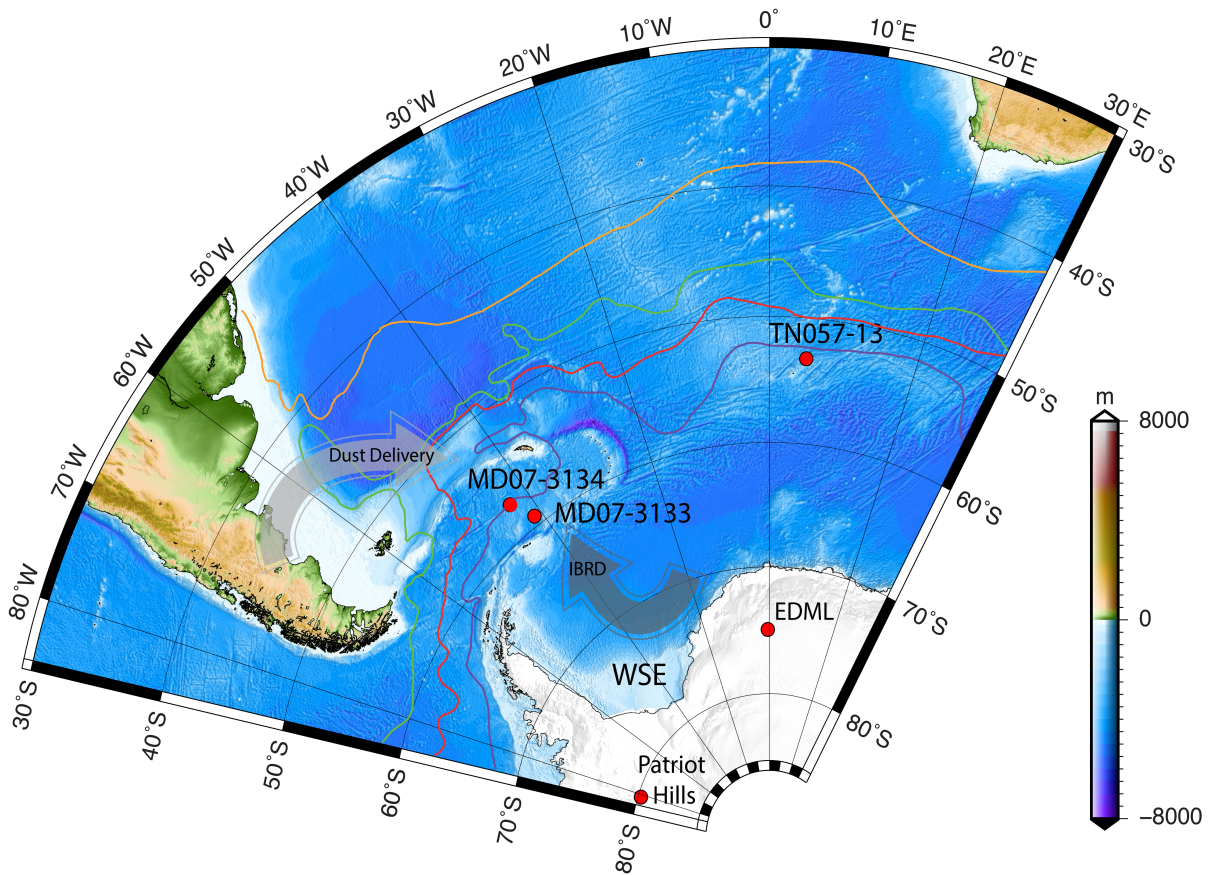
110 One striking feature of the LGT record is a 1,900 year-long-plateau in CO₂ concentration, when
111 CO₂ paused at a near-constant 240 ppm coinciding with the period of high latitude Southern
112 Hemisphere surface cooling, termed the Antarctic Cold Reversal (ACR; 14.6-12.7 kyr BP) (Pedro
113 et al., 2015). Whilst the rapid rises in CO₂ may be attributed to either terrestrial carbon feedbacks
114 or through shifts in the Intertropical Convergence Zone (ITCZ) that may have impacted ocean

115 circulation and the location and intensity of the Southern Hemisphere Westerlies (Bauska et al.,
116 2016), the enigmatic plateau between 14.6-12.7 kyr BP remains unexplained (Figure 1). In the
117 absence of clear mechanisms the need for well resolved palaeo-proxy reconstructions that may
118 shed light on causes of this plateau are needed, as it may help reveal new insights into the high-
119 latitude ocean's potential for carbon sequestration (Boyd et al., 2019). Here we exploit an
120 innovative new ice core record to reconstruct high-latitude environmental changes during the ACR
121 to gain new insights into the driver (s) of Southern Ocean carbon feedbacks during this important
122 transition.

123

124 The ACR was characterized by surface cooling across the mid to high-latitude Southern
125 Hemisphere (Fogwill and Kubik, 2005; McGlone et al., 2010; Pedro et al., 2015), coincident with
126 sustained warming across the Northern Hemisphere (the North Atlantic Bølling-Allerød
127 interstadial) (Jaccard et al., 2016; Marcott et al., 2014), abrupt global sea level rise (Fogwill et al.,
128 2017; Weber et al., 2014), and major disruptions to atmospheric and ocean circulation, and the
129 carbon cycle (Jaccard et al., 2016; Martínez-García et al., 2014; Schmitt et al., 2012). Whilst the
130 global sequence of events during the ACR is reasonably well known (Pedro et al., 2015), a clear
131 understanding of the drivers and impacts of contrasting polar climate changes on global CO₂ trends
132 has proved elusive due to the challenges in precisely aligning ice and marine records across this
133 period (Jaccard et al., 2016). In part this reflects the lack of well-resolved, high accumulation
134 marine sedimentary records from the high-latitude Southern Ocean. One crucial record in this
135 regard comes from marine sediment core TN057-13 (~53°S) (Anderson et al., 2009; Jaccard et al.,
136 2016) (Figure 2), which suggests that the ACR was characterized by reduced carbon sequestration
137 in the mid-latitudes (as measured by decreased biological productivity or export production

138 (Anderson et al., 2009; Gottschalk et al., 2016); Figure 1D), possibly the result of enhanced
139 stratification that decreased the vertical supply of nutrients across the high-nutrient, low-
140 chlorophyll (HNLC) sectors of the Southern Ocean during cooling (Anderson et al., 2009).
141 However, such a hypothesis is difficult to test in the absence of other well resolved, high-latitude
142 records of Southern Ocean productivity.



143
144 **Figure 2.** Location map of the South Atlantic sector of the Southern Ocean with the locations of
145 Patriot Hills in the Ellsworth Mountains, the EPICA Dronning Maud Land (EDML) ice core
146 (Wolff et al., 2006a), the Scotia Sea MD07-3134 core (Weber et al., 2014), and marine core
147 TN057-13 (Anderson et al., 2009) produced with GMT (Wessel, 1998). Locations of the southern
148 limb of the Antarctic Circumpolar Current (purple), the polar front (red), subantarctic front (green)
149 and the subtropical front (yellow) (Orsi et al., 1995).

150 Changes in Southern Ocean productivity polewards of TN057-13 are recorded within the highly-
151 resolved marine core MD07-3134, located at $\sim 59^{\circ}\text{S}$ in the Scotia Sea (Figure 1E; see
152 Supplementary Information) (Weber et al., 2014). In common with core TN057-13 this sequence
153 is exceptionally well resolved, with sedimentation rates of 20 to 200 cm/kyr (Weber et al., 2014).
154 Here we report opal burial rates from MD07-3134 used, after accounting for sediment focussing
155 with ^{230}Th normalisation (see Supplementary Information) (Meyer-Jacob et al., 2014), we estimate
156 changes in biological productivity (export production) at the site (Figure 1E). The reconstruction
157 suggests that whilst export production in the high-latitude Southern Ocean similarly increased
158 from ~ 17 ka, the trend was maintained through the ACR, in antiphase to records further north
159 (Anderson et al., 2009) (Figure 1 and Figure 2), suggesting that at high latitudes other driver(s) of
160 marine biological activity may have operated during this period. In the absence of a network of
161 highly resolved marine records from the high-latitude Southern Ocean that have been normalised
162 for sedimentation rate changes (through ^{230}Th normalisation (see Supplementary Information))
163 (Sprenk et al., 2013), we develop a new record of high-latitude surface ocean productivity using
164 the marine biomarkers and DNA analyses of picoplankton and nanoplankton from a highly-
165 resolved horizontal ice core from the Weddell Sea Embayment, Antarctica (Fogwill et al., 2017),
166 that captures regional-scale processes operating across the south Atlantic sector of the Southern
167 Ocean across the LGT (Figure 3) (Fogwill et al., 2017; Turney et al., 2013).

168 **Materials and methods**

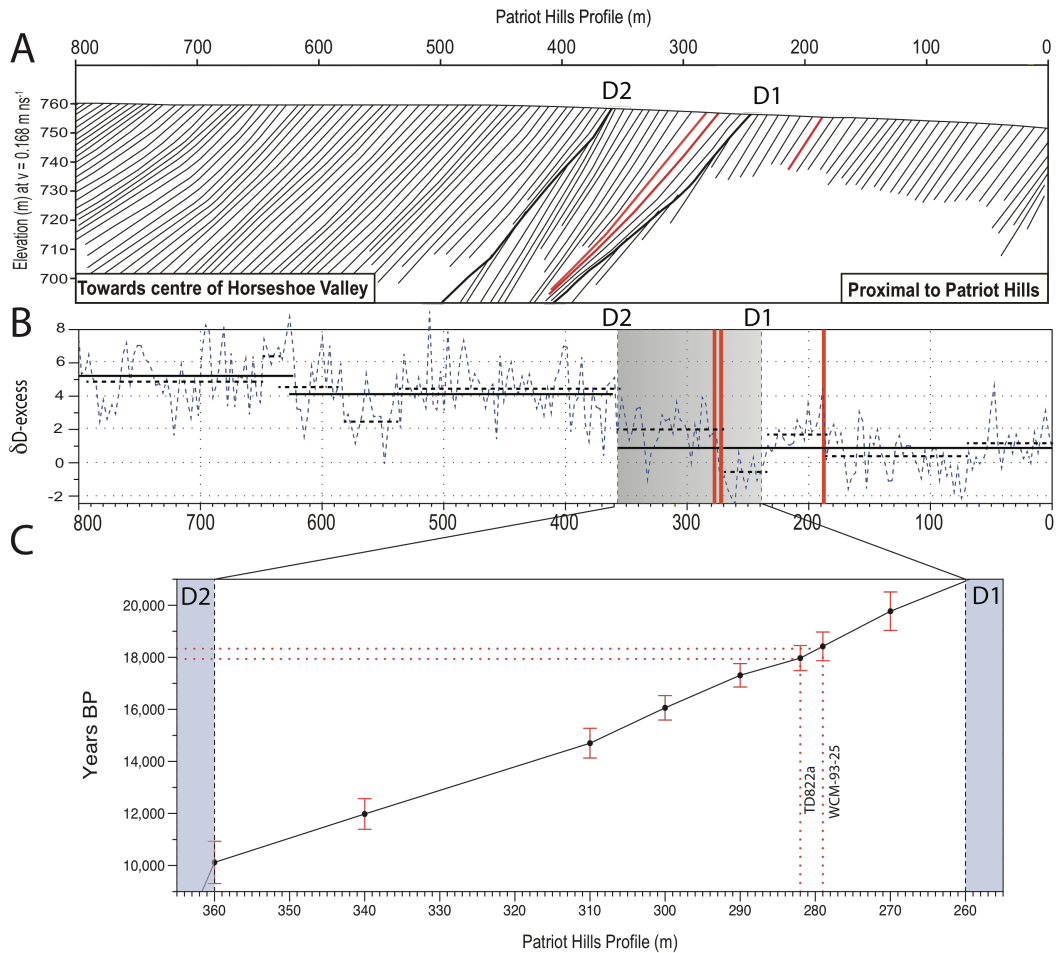
169 The ‘horizontal’ ice core record was obtained from the exposed blue ice area (BIA) at Patriot Hills
170 in Horseshoe Valley, Ellsworth Mountains (Figure 2) (Fogwill et al., 2017), which, in contrast to
171 many other BIA areas has not been mixed through ice flow (Fogwill et al., 2017; Winter et al.,
172 2016a). Horseshoe Valley is a locally-sourced compound glacier that is buttressed by, but

173 ultimately coalesces with, the Institute Ice Stream close to the contemporary grounding line of the
174 AIS making it the ideal site to build up a record of environmental and ice sheet change in this
175 sector of Antarctica (Fogwill et al., 2017). With contemporary snow accumulation at the site being
176 associated with low-pressure systems that have either tracked across the Weddell Sea from the
177 southern Atlantic Ocean, or that relate to blocking by the Antarctic Peninsula (Abram et al., 2007;
178 Reijmer et al., 1999; Turney et al., 2013), the site is ideally placed to record environmental changes
179 across the Scotia Sea, Weddell Sea and high-latitude South Atlantic (Figure 2).

180

181 The Patriot Hills record is chronologically constrained by multiple greenhouse gas species (CO₂,
182 CH₄ and N₂O) supported by geochemically identified volcanic (tephra) horizons (Figure 3 and
183 Supplementary Information), with increased sampling and more tephra's identified providing
184 tighter chronological control through the LGT building on previous studies (Fogwill et al., 2017).
185 The age model demonstrates that the BIA sequence spans from ~2.5 to 50 kyr BP, with two
186 unconformities (Discontinuities D1 and D2), that mark the build-up to (D1), and deglaciation from
187 (D2), the last glacial cycle (Figure 3) (Fogwill et al., 2017). High-resolution ground penetrating
188 radar (Winter et al., 2016b) and detailed analysis of trace gases and volcanic tephra horizons
189 (Fogwill et al., 2017) demonstrates that the conformable BIA layers or 'isochrons' between these
190 two unconformities span the period between ~11 to ~23 kyr BP (Figure 3C). Thus the horizontal
191 ice core captures a unique highly-resolved record of ice-sheet dynamics (Fogwill et al., 2017), in
192 an area of exceptionally slow moving ice, with no chronological breaks or unconformities across
193 the LGT (see Supplementary Information), providing an opportunity to obtain large volume ice
194 samples of known ages for innovative multiproxy biomarker analyses (Fogwill et al., 2017).

195



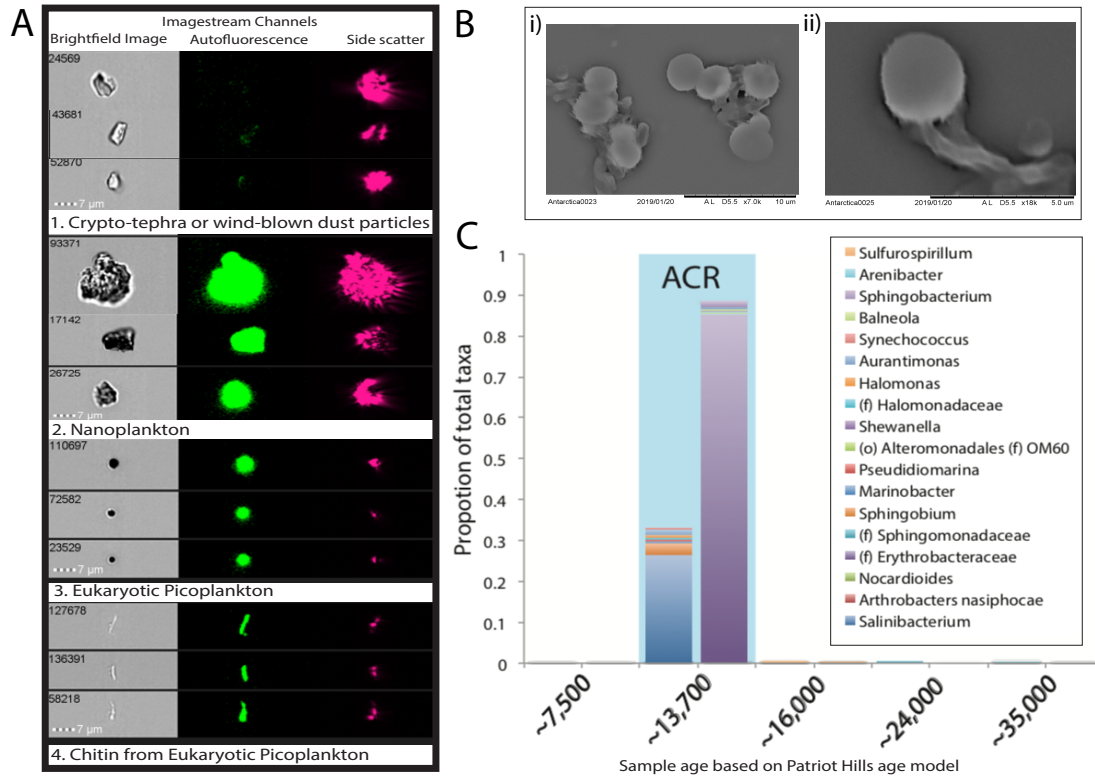
196

197 **Figure 3.** A. Schematic stratigraphic succession from Ground Penetrating Radar (GPR), across the
 198 Patriot Hills BIA, indicating ice accumulation punctuated by two periods of erosion (D1 and D2;
 199 thick black lines), and the position of tephras at 282m, 279m and 190m (red lines) across the profile
 200 (Fogwill et al., 2017). B. Dashed blue line represents $\delta\text{D-excess}$ across profile; solid horizontal
 201 black lines denote potential regime shifts across the profile at 99% confidence, and dashed black
 202 lines denote potential regime shifts across the profile at 95% confidence (Rodionov, 2004). C.
 203 Age-depth model based upon chronological control ties between D1 ~21 ka (21,000 years) and D2
 204 ~10 ka (10,000 years) as defined from volcanic ‘tephra’ horizons and most-likely age as derived
 205 from multiple trace gas comparison (CH_4 , CO_2 , N_2O ; see Supplementary Information (Fogwill et

206 al., 2017)).

207

208 To examine regional environmental responses through the LGT, fluorescent organic matter (fOM)
209 content and liquid chromatography organic carbon detection (LC-OCD) (Huber et al., 2011)
210 analysis of biomarkers was undertaken on LGT ice outcropping at the Patriot Hills BIA (see
211 Supplementary Information and Figure 4) (Huber et al., 2011). Detailed analysis of the
212 fluorescence emission spectra identified two protein-like components (Stedmon et al., 2003) in ice
213 throughout the profile. Due to their excitation-emission wavelengths, we can unambiguously
214 identify these fOM components as those widely reported in precipitation as TRYLIS and TYLIS:
215 tryptophan and tyrosine-like substances (Jørgensen et al., 2011; Parlanti et al., 2000) (see
216 Supplementary Information (Figure S2)). Whilst there are limited studies in ancient Antarctic ice
217 (D'Andrilli et al., 2016), past studies have demonstrated that a strong TRYLIS signal is found in
218 Antarctic snow and ice derived from precipitation from the marine environment (Barker et al.,
219 2013; Hood et al., 2009; King et al., 2019; Rohde et al., 2008; Smith et al., 2017).



220

221 **Figure 4. A.** Imaging Flow Cytometry (ImageSteam®) analysis highlights the four principal
 222 populations identified in ancient ice from the Patriot Hills BIA. **B.** SEM images of marine
 223 picoeukaryotes with tails (chitin) **C.** Microorganisms previously identified in marine seawater
 224 (teal) or marine sediments (light blue) are observed in samples from different sections of the Patriot
 225 Hills BIA. The proportion of the taxa from each core, given a specific extraction method
 226 (Powerlyzer left hand side, or CTAB, right hand side). The period defined by the ACR is
 227 represented by the blue box.

228

229 To unambiguously identify the source of the fOM signal and confirm our interpretation of a marine
 230 origin we apply Imaging Flow Cytometry (ImageSteam®) and Scanning Electron Microscopy
 231 (SEM) to ancient ice samples. Imaging Flow Cytometry reveals four significant populations
 232 preserved within ice from samples in the Patriot Hills BIA record (Figure 4A). The first is an

233 inorganic fraction ranging from $\sim 2\text{-}10\mu\text{m}$ in length, characterised by a flaky flat structure and no
234 autofluorescence, which we interpret as a mixture of crypto-tephra, and / or wind-blown dust. The
235 second population is composed of dark angular particles $\sim 5\text{-}12\mu\text{m}$ in length, that have a high
236 autofluorescence, and a 3-D structure evidenced from a strong ch006 (side scatter) signal, which
237 we classify as nanoplankton. The third population is characterised by spheroidal forms ranging in
238 diameter from $\sim 2\text{-}5\mu\text{m}$, that again have a high autofluorescence, and a 3-D structure evidenced
239 from a strong ch006 (side scatter) signal, which we identify as Eukaryotic picoplankton and
240 picoeukaryotes. Finally, a fourth population is characterised by elongate spicules or rods between
241 $2\text{-}10\mu\text{m}$, that have a high autofluorescence, and a 3-D structure evidenced from a strong ch006
242 (side scatter) signal, which we identify as Chitin, most likely related to the third population of
243 eukaryotic picoplankton and picoeukaryotes, an interpretation confirmed through SEM (Figure
244 4B). Beyond these four populations only a few other events were recorded, which were identified
245 as broken diatom frustules, which were characterised by a high autofluorescence, and a side scatter
246 signal (see Supplementary Information).

247

248 Of the populations identified through Imaging Flow Cytometry (ImageStream®) the eukaryotic
249 picoplankton and picoeukaryotes and Chitin populations made up most the made $\sim 56\%$ of the total,
250 with the non-fluorescent signal $\sim 12\%$, and finally $\sim 36\%$ of the signal being less than $<2\mu\text{m}$,
251 therefore unclassified at present (Classification of this fine particulate fraction is difficult due to
252 its small size. However, $\sim 20\%$ of events within this fraction are characteristic of picoeukaryotes
253 (displaying similar properties to eukaryotic picoplankton identified in the $> 2\mu\text{m}$ fraction, below).
254 The remaining 80% is comprised of 'elongate fluorescent rods' (likely chitin), and unclassified
255 angular and round particulate.

256

257 The fact that the picoplankton and picoeukaryotes populations ($>2\mu\text{m}$) were not recorded as one
258 population in the Imaging Flow Cytometry (ImageStream®) analysis was concerning, and likely
259 reflects the process of the flow cytometry, where sheath fluids run through the machine at the same
260 time as the sample – this focuses the sample in a steady stream, so that each ‘event’ can be analysed
261 individually. This effect, or possibly vortexing prior to analysis, may have disaggregated the
262 picoplankton and picoeukaryotes, separating the tails (chitin) from the spheroidal ‘body’ (see
263 Supplementary Information). To test this Scanning Electron Microscopy (SEM) was undertaken
264 on samples that had not been previously unfrozen or analysed. SEM imaging demonstrated
265 unambiguously that whole picoplankton and picoeukaryotes were present in the water samples
266 from ancient ice, complete with chitin (Figure 4B).

267

268 Having undertaken four independent yet mutually supportive biomarker approaches on ice samples
269 across the LGT from the Patriot Hills BIA we can conclude that marine biomarkers are present
270 throughout the profile. The location of the BIA, the unambiguous nature of the biomarker signal,
271 and the observation that marine regions have exceptionally low humic-like substances (HULIS)
272 content and relatively high TRY LIS content (Muller et al., 2008; Willey, 2000), indicates that the
273 primary source of fOM in the ice is from precipitation derived from the high-latitude Southern
274 Ocean (Abram et al., 2007; Reijmer et al., 1999; Turney et al., 2013). This interpretation is
275 supported by both independent LC-OCD and independent fluorescence techniques (see Figure 4
276 and Supplementary Information (Figure S2)), which fail to identify the presence of humic-like
277 substances in ice from the Patriot Hills BIA, ruling out either a terrestrial source of the fOM signal
278 or *in situ* secondary production (Smith et al., 2017) in the ancient ice which was recovered from

279 depth. Imaging Flow Cytometry (ImageStream®) identifies that the bulk of the fOM signal relates
280 to the presence of microscopic marine plankton, principally picoplankton and picoeukaryotes, but
281 also with nanoplankton populations up to $\sim 8\mu\text{m}$ in size.

282

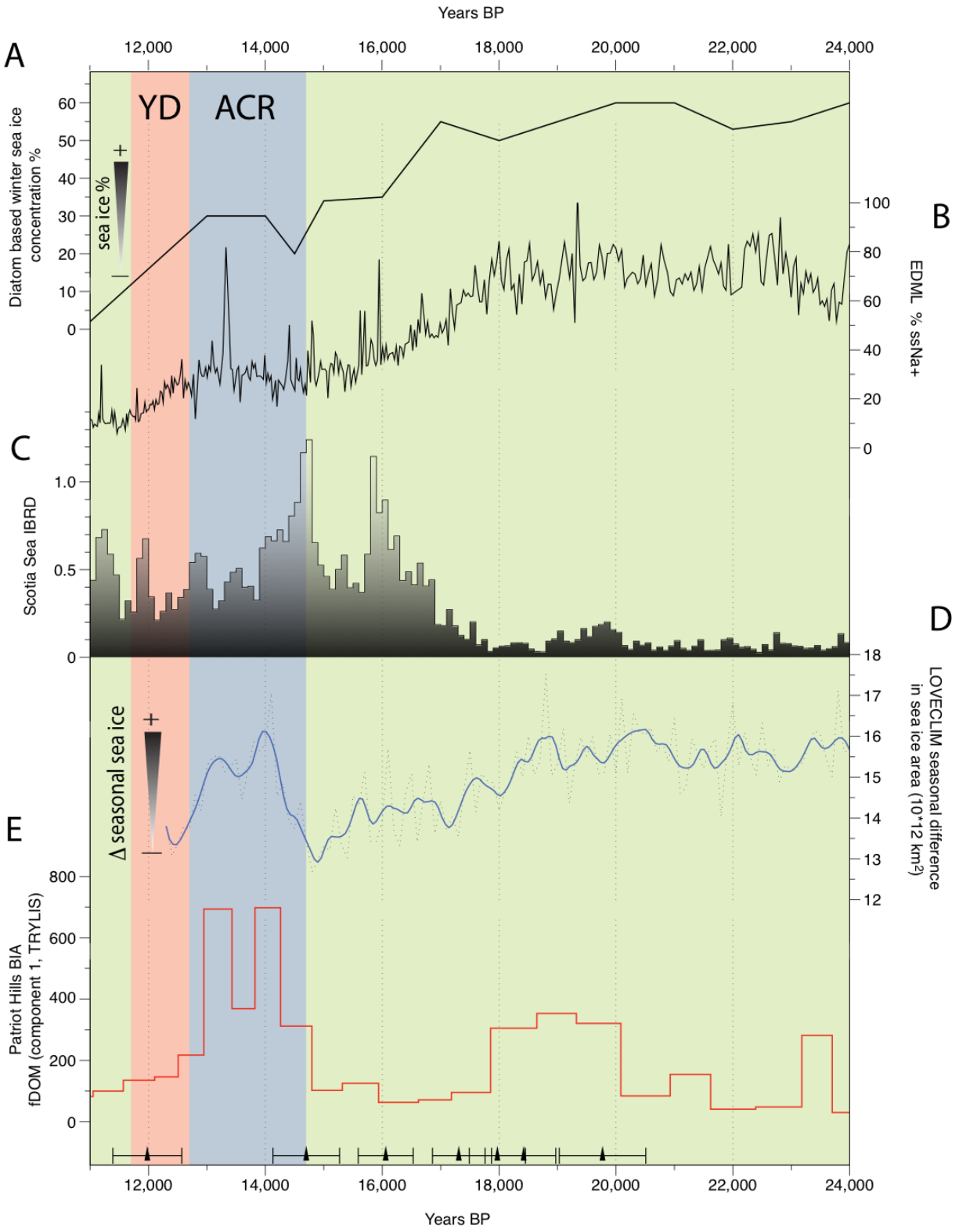
283 As recorded in contemporary mesoscale experiments picoplankton and picoeukaryotes form the
284 basis of the pelagic communities response to iron fertilisation in the high-latitude HLNC Southern
285 Ocean(Boyd et al., 2000), and are key to CO_2 draw down in the polar Southern Ocean(Boyd et al.,
286 2019). With Imaging Flow Cytometry and independent biomarker (fOM and LC-OCD) analysis
287 demonstrating that the TRYLIS and TYLIS components identified are a measure of picoplankton
288 and picoeukaryotes populations the fOM signal can be interpreted as a robust measure of Southern
289 Ocean productivity in the Weddell and Scotia Sea areas of the South Atlantic sector of the Southern
290 Ocean. With both the TRYLIS and TYLIS components being identified in the WAIS Divide
291 core(Rohde et al., 2008) and in the fOM signal in contemporary snow cores from the Patriot Hills
292 site that record the past decade (see Supplementary Information (Figures S1 and S2)), it provides a
293 measure of high-latitude surface marine productivity in this sector of the Southern Ocean that can
294 be linked to export production in the Southern Ocean (Boyd et al., 2000), a hypothesis testable
295 through the analysis of marine sediments from sites such as The Scotia Sea.

296

297 **Results**

298 By comparing the records of fOM across the LGT we observe a pronounced peak in these
299 biomarkers across the well-constrained ACR part of the Patriot Hills BIA sequence (Figure 5).
300 This change in fOM signal could reflect marked changes in precipitation source over the LGT;
301 however, regime shift analysis (Rodionov, 2004) on the deuterium-excess profile measured across

302 the LGT profile reveals no significant variability across the ACR, or the LGT, at either 99% or
303 95% confidence, indicating that the precipitation source remained constant (Figure 3C). The
304 implication is that the fOM signal reflects large relative variations in the concentration of TRYLIS
305 and TYLIS in the precipitation source region produced by the aerial transport of marine
306 microorganisms, principally nanoplankton, picoplankton and picoeukaryotes as identified through
307 ImageSteam®. In our analysis, we focus on the variation in the TRYLIS component, which makes
308 up highest percentage of the variance in fOM signal (83.33%: see Supplementary Information).
309 The fOM TRYLIS component, hence concentration of marine-derived nanoplankton,
310 picoplankton and picoeukaryotes, is highly variable across the BIA ice core record but has a
311 sustained high concentration through the ACR (Figure 5E).



313 **Figure 5.** Comparison of A. Diatom transfer function-based estimates of winter sea-ice
314 concentration (Esper and Gersonde, 2014), B. Sea salt (ssNa⁺) from EPICA Dronning Maud Land
315 (EDML) (Wolff et al., 2006a). C. Iceberg-rafted debris flux (IBRD; normalised 100-year average)
316 relative to Holocene from core MD07-3134 (Weber et al., 2014). D. Difference in seasonal extent
317 of Antarctic sea-ice area from LOVECLIM (Menviel et al., 2011) and E. fOM concentration
318 (Component 1; TRYLIS, raw data is represented by a solid red line). Vertical boxes indicate the
319 periods defined by the Antarctic Cold Reversal (ACR) (blue), the Younger Dryas (YD)
320 chronozone (11.7-12.7 ka) and black triangles represent the age tie points (derived from
321 geochemically identified volcanic horizons and trace gases, see Supplementary Information and
322 Figure S1) in this section of the Patriot Hills BIA (see Figure 3).

323

324 To further investigate the detail of the marine biomarker signals, large volume ice samples were
325 sampled across the LGT portion of the exposed BIA at Patriot Hills to extract ancient bacterial
326 DNA *in situ* by directly melting and filtering samples from specific time-horizons – a novel
327 approach to minimize the introduction of contaminants (see Supplementary Information) and
328 which enables us to obtain insights into the picoplankton, picoeukaryotes and nanoplankton
329 represented at a taxa level. 16S rRNA indexing reveals a marked ecological switch characterized
330 by the appearance of large numbers of halotolerant microorganisms commonly found in seawater
331 was observed during the ACR, coincident with the increase in fOM TRYLIS signal (Figure 4C
332 (see Supplementary Information (Tables S1 and S2)). Specifically, we found marine-associated
333 taxa, *Helicobacteraceae*, *Rhodobacteraceae*, *Marinobacter* and *Pseudidiomarina*, statistically
334 associated with the ACR period ($p < 0.038$), and observe a slight increase in species diversity
335 (predominantly marine taxa) compared to that observed during either the mid-Holocene or the

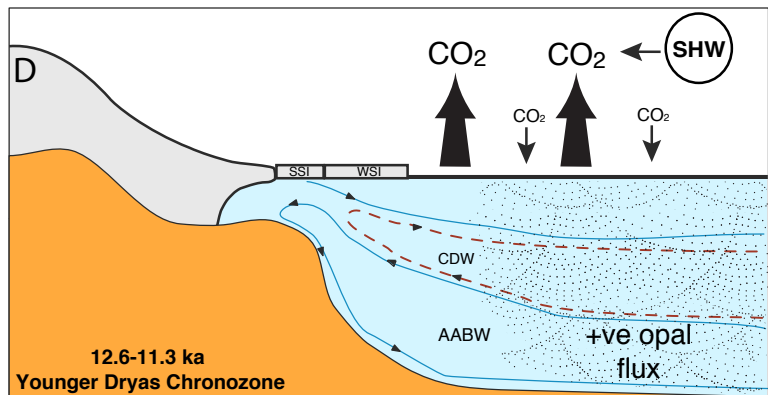
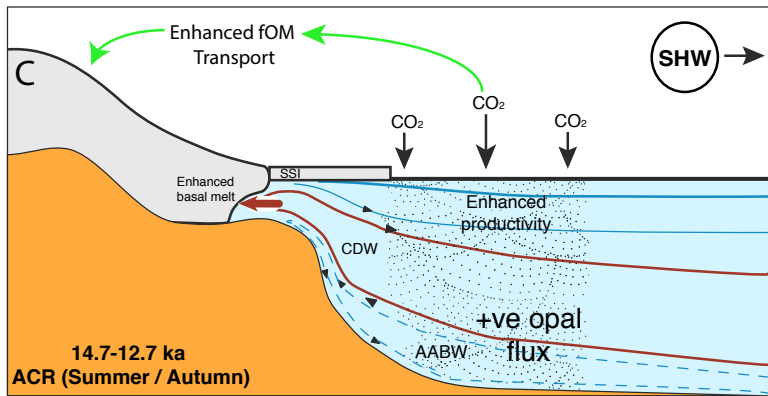
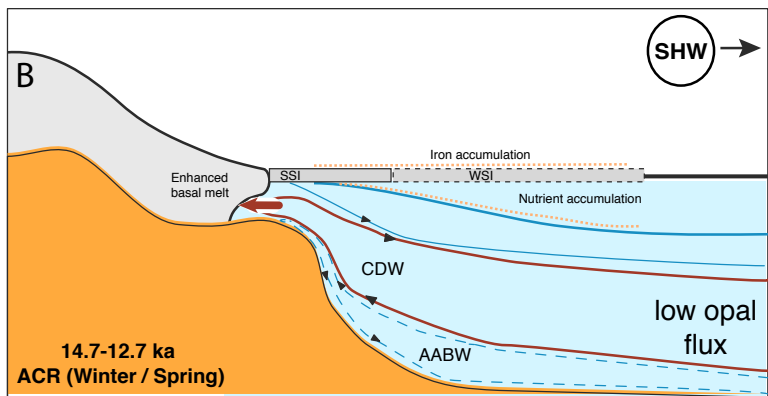
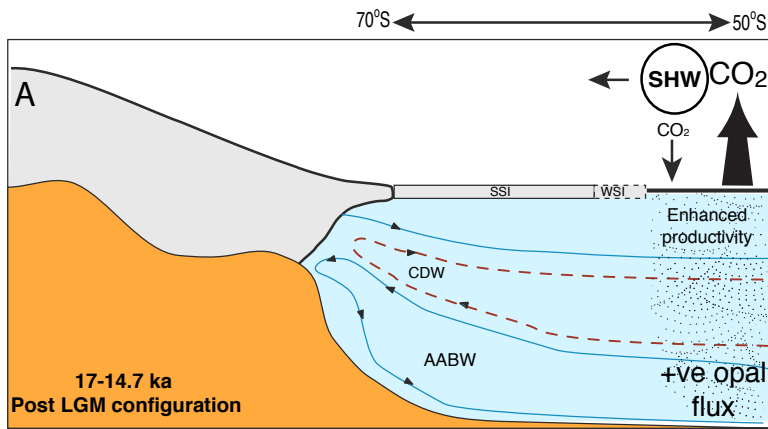
336 glacial samples from the Patriot Hills BIA sequence (Figure 5, Tables S1 and S2). Whilst the source
337 of this signal could have been from brine pools associated with the build-up of sea ice, we suggest,
338 based on the taxa identified, that the signal reflects an enhanced diversity and productivity from
339 open marine, or marginal sea ice zone. With five independent approaches (LC-OCD, Imaging
340 Flow Cytometry analysis, and the independent fOM and DNA) each pointing to enhanced marine
341 biological productivity in the high latitude South Atlantic sector of the Southern Ocean our results
342 infer that the ACR was a period of enhanced marine biological productivity. With the enhanced
343 picoplankton and picoeukaryotes signals derived from the surface precipitation source waters of
344 the HNLC Southern Ocean during the ACR, we suggest that there was a strengthening of the
345 biological pump which mirrored the effects of iron-fertilisation(Boyd et al., 2000) in this South
346 Atlantic Sector of the Southern Ocean, a finding that supports the enhanced export production
347 recorded in marine sediments from the Scotia Sea (Figure 1E) (Weber et al., 2014).

348

349 **Discussion**

350 To reconcile the apparent conflict between the increase in marine productivity recorded in marine
351 sediments from the Scotia Sea and the Patriot Hills ice core with the decrease reported further
352 north in the South Atlantic (Anderson et al., 2009; Jaccard et al., 2016) during the ACR, we
353 compare our record of marine biomarkers (fOM) captured in ice with potential drivers of Southern
354 Ocean productivity. We compare available records of iceberg rafted debris (IBRD; a proxy for
355 Antarctic iceberg discharge) (Weber et al., 2014)), sea salt sodium ($ssNa^+$) from the EDML ice
356 core (a proxy for sea-ice extent) (Wolff et al., 2006b), proxy sea-ice reconstructions (Abelmann et
357 al., 2015; Esper and Gersonde, 2014) to investigate possible physical drivers of enhanced
358 productivity, and we compare independent transient modelling experiments using LOVECLIM

359 that include fresh water hosing in the Ross and Weddell seas (Menviel et al., 2011) (Figure 5; and
360 Supplementary Information). Comparison between these records and the BIA LGT record between
361 ~24 and ~14.6 kyr BP indicate weak relationships between marine biological productivity (using
362 opal flux as a measure of export production), sea-ice expansion, atmospheric CO₂ variability and
363 the peak in marine derived biomarkers (fOM), agreeing with previous studies (Figure 5) (Collins
364 et al., 2012). This contrasts with the period defined by the ACR, where we observe a strong
365 relationship between marine fOM in the Patriot Hills BIA, increased production of biogenic opal
366 in the Scotia Sea, and the extended atmospheric CO₂ plateau across the ACR (Figures 1 and 5).
367 Given that this increase in marine productivity seen in the Scotia Sea during the ACR is not
368 apparent in mid-latitude marine records (Figure 2)(Anderson et al., 2009; Jaccard et al., 2016), we
369 focus on possible high-latitude drivers of CO₂ exchange: iron fertilization from enhanced IBRD
370 flux (Duprat et al., 2016), a reduction in Antarctic Bottom Water (AABW) formation due to
371 enhanced freshwater flux (Fogwill et al., 2015; Golledge et al., 2014; Menviel et al., 2010), and
372 sea-ice feedbacks (Abelmann et al., 2015) (Figure 6).



374 **Figure 6.** Schematic cross section of the mid to high latitude Southern Ocean. A. Post-Last Glacial
375 Maximum (LGM) configuration with southerly displacement of the Southern Hemisphere
376 Westerlies (SHW), depicting enhanced overturning of mid-latitude Southern Ocean between ~17
377 ka- 14.7 ka as suggested by opal flux (Anderson et al., 2009). B. Antarctic Cold Reversal with
378 enhanced intrusion of Circumpolar Deepwater (CDW) onto Antarctic shelf areas. Austral winter /
379 spring, depicts marked winter sea-ice expansion (WSI), northwards migration of the SHW, with
380 stratification and deepening of the mixed layer allowing ‘nutrient refuelling’ from deeper nutrient-
381 enriched ocean and reduction in AABW formation at high-latitudes (Abelmann et al., 2015). C.
382 Antarctic Cold Reversal (austral summer/autumn), extensive WSI break up enhancing marine
383 primary productivity, from light and iron fertilization in a warming ocean leading to enhanced CO₂
384 drawdown in high-latitude HNLC Southern Ocean. D. Younger Dryas chronozone mid-latitude
385 overturning reinvigorated leading to degassing of old carbon, and enhanced opal flux across the
386 Southern Ocean.

387

388 IBRD contains high concentrations of bioavailable iron, making iceberg melt a potential source
389 for increased primary productivity and carbon sequestration through fertilization across the HNLC
390 regions of the high-latitude Southern Ocean (Duprat et al., 2016). Intriguingly, despite significant
391 evidence for potential enhanced iron fertilization of the Southern Ocean through increased delivery
392 of IBRD at around 20-19 kyr BP and 17-16 kyr BP (Weber et al., 2014), there does not seem to be
393 a strong biological response in the Patriot Hills fOM or Scotia Sea opal flux records (Figures 2 and
394 5), suggesting enhanced IRBD influx did not lead to enhanced high-latitude marine export
395 production.

396

397 Alternatively, an increase in meltwater flux and reduction in the rate of AABW formation during
398 the ACR (Golledge et al., 2014; Menviel et al., 2011; Menviel et al., 2016; Weber et al., 2014)
399 may have increased stratification and carbon sequestration across the high-latitude Southern
400 Ocean. Published analysis has demonstrated that there was significant ice-sheet drawdown across
401 the Weddell Sea Embayment at this time (Fogwill et al., 2017; Weber et al., 2014), suggesting that
402 influx of meltwater could have triggered stratification, and substantial circulation changes across
403 the broader Southern Ocean, magnified by associated shifts in the intensity and/or location of
404 surface westerly air flow (Anderson et al., 2009; Fogwill et al., 2017; Hogg et al., 2016; Jaccard
405 et al., 2016). This interpretation is supported by independent ice-sheet and Earth system modelling
406 experiments (Menviel et al., 2011; Weber et al., 2014). However, the disparity in the opal flux
407 records between marine cores from the mid-latitude South Atlantic (Anderson et al., 2009) and
408 Scotia Sea, suggests that the enhanced export production was focussed on the high-latitude South
409 Atlantic during the ACR (Figure 1).

410

411 An alternative mechanism that could enhance marine productivity at the high-latitudes involves
412 sea-ice feedbacks. Recent studies of full glacial conditions suggest that reduced surface–deep
413 ocean exchange and enhanced nutrient consumption by phytoplankton in the Southern Ocean may
414 have lowered atmospheric CO₂ (Abelmann et al., 2015; Collins et al., 2012). During the austral
415 winter, sea-ice expansion allowed the mixed layer to deepen, ‘refuelling’ the surface ocean with
416 nutrients from the deep ocean reservoir, and enhancing near-surface productivity and export
417 production during the break up of sea ice in the subsequent summer. This process was likely
418 amplified by the addition of iron from sea-ice melt and breakup in the post-glacial HNLC ocean,
419 and possibly seasonal temperature changes and CaCO₃ dissolution (Delille et al., 2014).

420

421 The strong marine fOM signal preserved in the Patriot Hills BIA coincides with Southern
422 Hemisphere surface ocean and atmosphere cooling during the ACR (Figure 5). Proxy records and
423 transient Earth system modelling (Menviel et al., 2011) suggest the highest seasonal variability in
424 sea-ice extent across the LGT took place during the ACR (with greatest extent during winter and
425 spring) (Figure 5), implying these sea-ice feedbacks were amplified across this period (Figure 6).
426 The conditions contrast markedly in the periods immediately prior to (Figure 6A) and following
427 (Figure 6D) the ACR, when the seasonal sea ice zone was relatively less variable (Figure 5), the
428 high-latitude Southern Ocean less stratified (Golledge et al., 2014; Menviel et al., 2011; Weber et
429 al., 2014), and the location of the Intertropical Convergence Zone (ITCZ) and mid-latitude
430 Southern Hemisphere Westerlies were relatively further south (Figure 2). Set against a backdrop
431 of a warming ocean during the LGT this likely created ideal conditions for enhanced Southern
432 Ocean productivity in the high-latitude Southern Ocean, especially in sectors of the South Atlantic
433 such as the Weddell and Scotia seas.

434

435 Comparison between our continuous Scotia Sea opal flux record (Weber et al., 2014) and the
436 Patriot Hills BIA fOM record suggests that we are capturing a high-latitude signal of enhanced
437 surface marine primary productivity caused by marked seasonal sea-ice variability during the
438 ACR, a period characterised by a sustained atmospheric CO₂ plateau (Jaccard et al., 2016; Marcott
439 et al., 2014; Schmitt et al., 2012). During the ACR, most marine records across the mid-latitudes
440 suggest the biological pump in the Southern Ocean weakened, in apparent contradiction of the
441 plateau in atmospheric CO₂ at that time (Figure 2). Our results indicate that despite low dust input
442 (Figure 2), and surface cooling across subantarctic waters during the ACR, marked variability in

443 sea-ice extent resulted in increased seasonal surface productivity in the HNLC waters of the high-
444 latitude South Atlantic sector of the Southern Ocean in comparison to periods prior to and
445 following this event (Figure 5). We suggest that increased seasonal marine primary productivity
446 in fact enhanced the Southern Ocean organic carbon pump, increasing carbon drawdown (and
447 leading to enhanced export production) (Figure 6). Whilst other mechanisms may have played a
448 part in the 1,900 year-long ACR CO₂ plateau – including iron fertilization, cool Southern Ocean
449 surface temperatures and possibly reductions in the rate of AABW formation – the potential that
450 seasonal Southern Ocean sea-ice feedbacks in the South Atlantic sector of the high-latitude
451 Southern Ocean may have contributed to a slowdown in the rate of CO₂ rise during the ACR is a
452 significant observation that has implications for our understanding of the role of the Southern
453 Ocean in global carbon dynamics. Crucially, our results imply that during periods of Southern
454 Ocean sea-ice expansion, high variability in winter and summer sea-ice extent may result in
455 enhanced carbon sequestration as seen recently , providing a negative feedback during periods of
456 rising CO₂, a finding that requires detailed assessment given contemporary Antarctic sea ice
457 changes (Barnes, 2015).

458

459 **Acknowledgments:** CJF, CSMT, LM, NRG, LSW and AC are supported by their respective
460 Australian Research Council (ARC) and Royal Society of NZ fellowships, and CJF and AC thanks
461 Keele University for a Research Development Award that underpinned this research at Keele
462 University ICELAB and Exeter University. Fieldwork was undertaken under ARC Linkage Project
463 (LP120200724), supported by Linkage Partner Antarctic Logistics and Expeditions whose support
464 we gratefully acknowledge. CSIRO's contribution was supported in part by the Australian Climate
465 Change Science Program (ACCSP), an Australian Government Initiative. SMD acknowledges

466 financial support from Coleg Cymraeg Cenedlaethol and the European Research Council (ERC
467 grant agreement no. 25923). MEW acknowledges support from the Deutsche
468 Forschungsgemeinschaft (grant We2039/8-1). The data reported in this paper are archived on the
469 NOAA Paleoclimatology website. There are no competing interests.

470

471 **Author contribution:** CJF, CSMT, AB and AC conceived this research. CJF, CSMT, AB, MEW,
472 DE, MR DPT, TDvO, ADM, MAJC, SD, MB, NCM, JV, AR, LM, HM, CM, JY, MM, AC, MH,
473 AP, JL, LSW and AC undertook analysis and sampling. CJF, CSMT, AB, MEW and AC wrote
474 the manuscript with input from all the authors.

475

476 **Data availability:** The Patriot Hills δd and $\delta^{18}O$ isotope data, and the age model is available at
477 National Oceanic and Atmospheric Administration Paleoclimatology Database
478 (<https://www.ncdc.noaa.gov/paleo/study/21691>), and the data from core MD07-3134 are available
479 at <http://dx.doi.org/10.1594/PANGAEA.819646>. The biomarker and DNA data will be made
480 available upon publication through the NOAA archive.

481

482 **Additional Information:**

483 The authors declare no competing interests. Supplementary information accompanies this paper at
484 www.xxxxxxx. Correspondence and requests for materials should be addressed to C.J.F.
485 c.j.fogwill@keele.ac.uk.

486

487

488

489

490

491

492

493 **References**

- 494 Abelmann, A., Gersonde, R., Knorr, G., Zhang, X., Chaplignin, B., Maier, E., Esper, O.,
 495 Friedrichsen, H., Lohmann, G., Meyer, H., and Tiedemann, R., 2015, The seasonal sea-
 496 ice zone in the glacial Southern Ocean as a carbon sink: *Nature Communications*, v. 6, p.
 497 8136.
- 498 Abram, N. J., Mulvaney, R., Wolff, E. W., and Mudelsee, M., 2007, Ice core records as sea ice
 499 proxies: An evaluation from the Weddell Sea region of Antarctica: *Journal of*
 500 *Geophysical Research*, v. 112, no. D15101.
- 501 Anderson, R. F., Ali, S., Bradtmiller, L. I., Nielsen, S. H. H., Fleisher, M. Q., Anderson, B. E.,
 502 and Burckle, L. H., 2009, Wind-Driven Upwelling in the Southern Ocean and the
 503 Deglacial Rise in Atmospheric CO₂: *Science*, v. 323, no. 5920, p. 1443-1448.
- 504 Barker, J. D., Dubnick, A., Lyons, W. B., and Chin, Y.-P., 2013, Changes in Dissolved Organic
 505 Matter (DOM) Fluorescence in Proglacial Antarctic Streams: *Arctic, Antarctic and*
 506 *Alpine Research*, v. 45, no. 3, p. 305-317.
- 507 Barnes, D. K. A., 2015, Antarctic sea ice losses drive gains in benthic carbon drawdown: *Current*
 508 *Biology*, v. 25, no. 18, p. R789-R790.
- 509 Bauska, T. K., Baggenstos, D., Brook, E. J., Mix, A. C., Marcott, S. A., Petrenko, V. V.,
 510 Schaefer, H., Severinghaus, J. P., and Lee, J. E., 2016, Carbon isotopes characterize rapid
 511 changes in atmospheric carbon dioxide during the last deglaciation: *Proceedings of the*
 512 *National Academy of Sciences*, v. 113, no. 13, p. 3465-3470.
- 513 Boyd, P. W., Claustre, H., Levy, M., Siegel, D. A., and Weber, T., 2019, Multi-faceted particle
 514 pumps drive carbon sequestration in the ocean: *Nature*, v. 568, no. 7752, p. 327-335.
- 515 Boyd, P. W., Watson, A. J., Law, C. S., Abraham, E. R., Trull, T., Murdoch, R., Bakker, D. C.
 516 E., Bowie, A. R., Buesseler, K. O., Chang, H., Charette, M., Croot, P., Downing, K.,
 517 Frew, R., Gall, M., Hadfield, M., Hall, J., Harvey, M., Jameson, G., LaRoche, J.,
 518 Liddicoat, M., Ling, R., Maldonado, M. T., McKay, R. M., Nodder, S., Pickmere, S.,
 519 Pridmore, R., Rintoul, S., Safi, K., Sutton, P., Strzeppek, R., Tanneberger, K., Turner, S.,
 520 Waite, A., and Zeldis, J., 2000, A mesoscale phytoplankton bloom in the polar Southern
 521 Ocean stimulated by iron fertilization: *Nature*, v. 407, p. 695.
- 522 Butterworth, B. J., and Miller, S. D., 2016, Air-sea exchange of carbon dioxide in the Southern
 523 Ocean and Antarctic marginal ice zone. : *Geophysical Research Letters*, v. 43, p. 7223-
 524 7230.
- 525 Collins, L. G., Pike, J., Allen, C. S., and Hodgson, D. A., 2012, High-resolution reconstruction of
 526 southwest Atlantic sea-ice and its role in the carbon cycle during marine isotope stages 3
 527 and 2: *Paleoceanography*, v. 27, no. 3, p. PA3217.
- 528 D'Andrilli, J., Foreman, C. M., Sigl, M., Priscu, J. C., and McConnell, J. R., 2016, A 21,000 year
 529 record of organic matter quality in the WAIS Divide ice core: *Clim. Past Discuss.*, v.
 530 2016, p. 1-15.
- 531 Delille, B., Vancoppenolle, M., Geilfus, N.-X., Tilbrook, B., Lannuzel, D., Schoemann, V.,
 532 Becquevort, S., Carnat, G., Delille, D., Lancelot, C., Chou, L., Dieckmann, G. S., and
 533 Tison, J.-L., 2014, Southern Ocean CO₂ sink: The contribution of the sea ice: *Journal of*
 534 *Geophysical Research: Oceans*, v. 119, no. 9, p. 6340-6355.
- 535 Duprat, L. P. A. M., Bigg, G. R., and Wilton, D. J., 2016, Enhanced Southern Ocean marine
 536 productivity due to fertilization by giant icebergs: *Nature Geosci*, v. 9, p. 219-221.

537 Esper, O., and Gersonde, R., 2014, New tools for the reconstruction of Pleistocene Antarctic sea
538 ice: *Palaeogeography, Palaeoclimatology, Palaeoecology*, v. 399, p. 260-283.

539 Fogwill, C., Turney, C., Golledge, N., Etheridge, D., Rubino, M., Thornton, D., Baker, A.,
540 Woodward, J., Winter, K., and Van Ommen, T., 2017, Antarctic ice sheet discharge
541 driven by atmosphere-ocean feedbacks at the Last Glacial Termination: *Scientific reports*,
542 v. 7, p. 39979.

543 Fogwill, C. J., and Kubik, P. W., 2005, A glacial stage spanning the Antarctic Cold Reversal in
544 Torres del Paine (51 degrees S), Chile, based on preliminary cosmogenic exposure ages:
545 *Geografiska Annaler Series a-Physical Geography*, v. 87A, no. 2, p. 403-408.

546 Fogwill, C. J., Phipps, S. J., Turney, C. S. M., and Golledge, N. R., 2015, Sensitivity of the
547 Southern Ocean to enhanced regional Antarctic ice sheet meltwater input: *Earth's Future*,
548 v. 3, no. 10, p. 317-329.

549 Golledge, N. R., Menviel, L., Carter, L., Fogwill, C. J., England, M. H., Cortese, G., and Levy,
550 R. H., 2014, Antarctic contribution to meltwater pulse 1A from reduced Southern Ocean
551 overturning: *Nat Commun*, v. 5.

552 Gottschalk, J., Skinner, L. C., Lippold, J., Vogel, H., Frank, N., Jaccard, S. L., and Waelbroeck,
553 C., 2016, Biological and physical controls in the Southern Ocean on past millennial-scale
554 atmospheric CO₂ changes.: *Nat Commun*, v. 7, no. 11539.

555 Hewitt, A. J., Booth, B. B. B., Jones, C. D., Robertson, E. S., Wiltshire, A. J., Sansom, P. G.,
556 Stephenson, D. B., and Yip, S., 2016, Sources of uncertainty in future projections of the
557 carbon cycle.: *Journal of Climate*, v. 29, p. 7203-7213.

558 Hogg, A., Southon, J., Turney, C., Palmer, J., Bronk Ramsey, C., Fenwick, P., Boswijk, G.,
559 Friedrich, M., Helle, G., Hughen, K., Jones, R., Kromer, B., Noronha, A., Reynard, L.,
560 Staff, R., and Wacker, L., 2016, Punctuated shutdown of Atlantic Meridional Overturning
561 Circulation during the Greenland Stadial 1: *Scientific Reports*, v. 6, no. 25902.

562 Hood, E., Fellman, J., Spencer, R. G. M., Hernes, P. J., Edwards, R., D'Amore, D., and Scott,
563 D., 2009, Glaciers as a source of ancient and labile organic matter to the marine
564 environment: *Nature*, v. 462, no. 7276, p. 1044-1047.

565 Huber, S. A., Balz, A., Abert, M., and Pronk, W., 2011, Characterisation of aquatic humic and
566 non-humic matter with size-exclusion chromatography – organic carbon detection –
567 organic nitrogen detection (LC-OCD-OND): *Water Research*, v. 45, no. 2, p. 879-885.

568 Jaccard, S. L., Galbraith, E. D., Martínez-García, A., and Anderson, R. F., 2016, Covariation of
569 deep Southern Ocean oxygenation and atmospheric CO₂ through the last ice age: *Nature*,
570 v. 530, p. 207-210.

571 Jaccard, S. L., Hayes, C. T., Martínez-García, A., Hodell, D. A., Anderson, R. F., Sigman, D. M.,
572 and Haug, G. H., 2013, Two Modes of Change in Southern Ocean Productivity Over the
573 Past Million Years: *Science*, v. 339, no. 6126, p. 1419-1423.

574 Jørgensen, L., Stedmon, C. A., Kragh, T., Markager, S., Middelboe, M., and Søndergaard, M.,
575 2011, Global trends in the fluorescence characteristics and distribution of marine
576 dissolved organic matter: *Marine Chemistry*, v. 126, no. 1, p. 139-148.

577 King, A., Wolff, E., Thomas, E., Kalberer, M., Giorio, C., and MargitSchwikowski, 2019, Novel
578 organic compounds in ice cores for use in paleoclimatereconstruction: *Geophysical
579 Research Abstracts*, v. EGU General Assembly 2019, no. CL1.11/CR5.6

580 Le Quéré, C., Rödenbeck, C., Buitenhuis, E. T., Conway, T. J., Langenfelds, R., Gomez, A.,
581 Labuschagne, C., Ramonet, M., Nakazawa, T., Metz, N., Gillett, N., and Heimann, M.,

2007, Saturation of the Southern Ocean CO₂ sink due to recent climate change. : Science, v. 316, p. 1735-1738.

Marcott, S. A., Bauska, T. K., Buizert, C., Steig, E. J., Rosen, J. L., Cuffey, K. M., Fudge, T. J., Severinghaus, J. P., Ahn, J., Kalk, M. L., McConnell, J. R., Sowers, T., Taylor, K. C., White, J. W. C., and Brook, E. J., 2014, Centennial-scale changes in the global carbon cycle during the last deglaciation: Nature, v. 514, no. 7524, p. 616-619.

Marshall, J., and Speer, K., 2012, Closure of the meridional overturning circulation through Southern Ocean upwelling. : Nature Geoscience, v. 5, p. 171-180.

Martínez-García, A., Sigman, D. M., Ren, H., Anderson, R. F., Straub, M., Hodell, D. A., Jaccard, S. L., Eglinton, T. I., and Haug, G. H., 2014, Iron Fertilization of the Subantarctic Ocean During the Last Ice Age: Science, v. 343, no. 6177, p. 1347-1350.

McGlone, M. S., Turney, C. S. M., Wilmshurst, J. M., Renwick, J., and Pahnke, K., 2010, Divergent trends in land and ocean temperature in the Southern Ocean over the past 18,000 years: Nature Geosci, v. 3, no. 9, p. 622-626.

Menviel, L., A. Timmermann, O. Elison Timm, and Mouchet, A., 2011, Deconstructing the Last Glacial Termination: the role of millennial and orbital-scale forcings: Quaternary Science Reviews, v. 30, p. 1155-1172.

Menviel, L., J. Yu, F. Joos, A. Mouchet, K. J. Meissner, and England, M. H., 2016, Poorly ventilated deep ocean at the Last Glacial Maximum inferred from carbon isotopes: A data-model comparison study.: Paleoceanography, v. 31.

Menviel, L., Timmermann, A., Timm, O. E., and Mouchet, A., 2010, Climate and biogeochemical response to a rapid melting of the West Antarctic Ice Sheet during interglacials and implications for future climate: Paleoceanography, v. 25, no. 4, p. PA4231.

Meyer-Jacob, C., Vogel, H., Boxberg, F., Rosén, P., Weber, M., and Bindler, R., 2014, Independent measurement of biogenic silica in sediments by FTIR spectroscopy and PLS regression: Journal of Paleolimnology, v. 52, no. 3, p. 245-255.

Monnin, E., Indermöhle, A., Dällenbach, A., Flückiger, J., Stauffer, B., Stocker, T. F., Raynaud, D., and Barnola, J.-M., 2001, Atmospheric CO₂ Concentrations over the Last Glacial Termination: Science, v. 291, no. 5501, p. 112-114.

Muller, C. L., Baker, A., Hutchinson, R., Fairchild, I. J., and Kidd, C., 2008, Analysis of rainwater dissolved organic carbon compounds using fluorescence spectrometry. : Atmospheric Environment, v. 34, p. 8036-8045.

Orsi, A. H., III, T. W., and W. D. Nowlin, J., 1995, On the meridional extent and fronts of the Antarctic Circumpolar Current,: Deep-Sea Research, v. 1, no. 42, p. 641-673.

Parlanti, E., Wörz, K., Geoffroy, L., and Lamotte, M., 2000, Dissolved organic matter fluorescence spectroscopy as a tool to estimate biological activity in a coastal zone submitted to anthropogenic inputs: Organic Geochemistry, v. 31, no. 12, p. 1765-1781.

Pedro, J. B., Bostock, H. C., Bitz, C. M., He, F., Vandergoes, M. J., Steig, E. J., Chase, B. M., Krause, C. E., Rasmussen, S. O., Markle, B. R., and Cortese, G., 2015, The spatial extent and dynamics of the Antarctic Cold Reversal: Nature Geosci, v. 9, p. 51-55

Reijmer, C. H., Greuell, W., and Oerlemans, J., 1999, The annual cycle of meteorological variables and the surface energy balance on Berkner Island, Antarctica,: Ann. Glaciol., v. 29, p. 49-54.

627 Rodionov, S. N., 2004, A sequential algorithm for testing climate regime shifts: *Geophys. Res.*
628 *Letts.*, v. 31, no. L09204.

629 Rohde, R. A., Price, P. B., Bay, R. C., and Bramall, N. E., 2008, *In situ* microbial
630 metabolism as a cause of gas anomalies in ice: *Proceedings of the National Academy of*
631 *Sciences*, v. 105, no. 25, p. 8667-8672.

632 Schmitt, J., Schneider, R., Elsig, J., Leuenberger, D., Lourantou, A., Chappellaz, J., Köhler, P.,
633 Joos, F., Stocker, T. F., Leuenberger, M., and Fischer, H., 2012, Carbon Isotope
634 Constraints on the Deglacial CO₂ Rise from Ice Cores: *Science*, v. 336, no. 6082, p. 711-
635 714.

636 Smith, H. J., Foster, R. A., McKnight, D. M., Lisle, J. T., Littmann, S., Kuypers, M. M. M., and
637 Foreman, C. M., 2017, Microbial formation of labile organic carbon in Antarctic glacial
638 environments: *Nature Geosci*, v. 10, no. 5, p. 356-359.

639 Sprenk, D., Weber, M. E., Kuhn, G., Rosén, P., Frank, M., Molina-Kescher, M., Liebetrau, V.,
640 and Röhling, H.-G., 2013, Southern Ocean bioproductivity during the last glacial cycle –
641 new decadal-scale insight from the Scotia Sea: *Geological Society, London, Special*
642 *Publications*, v. 381, no. 1, p. 245-261.

643 Stedmon, C. A., Markager, S., and Bro, R., 2003, Tracing dissolved organic matter in aquatic
644 environments using a new approach to fluorescence spectroscopy.: *Marine Chemistry*, v.
645 82, p. 239–254.

646 Toggweiler, J. R., Russell, J. L., and Carson, S. R., 2006, Midlatitude westerlies, atmospheric
647 CO₂, and climate change during the ice ages: *Paleoceanography*, v. 21, no. 2.

648 Turney, C. S. M., Fogwill, C. J., Van Ommen, T. D., Moy, A. D., Etheridge, D., Rubino, M.,
649 Curran, M. A. J., and A., R., 2013, Late Pleistocene and early Holocene change in the
650 Weddell Sea: a new climate record from the Patriot Hills, Ellsworth Mountains, West
651 Antarctica: *Journal of Quaternary Science*, v. 28, no. 7, p. 697-704.

652 Turney, C. S. M., Palmer, J., Hogg, A., Fogwill, C. J., Jones, R. T., Bronk Ramsey, C., Fenwick,
653 P., Grierson, P., Wilmshurst, J., O'Donnell, A., Thomas, Z. A., and Lipson, M., 2016,
654 Multidecadal variations in Southern Hemisphere atmospheric ¹⁴C: Evidence against a
655 Southern Ocean sink at the end of the Little Ice Age CO₂ anomaly: *Global*
656 *Biogeochemical Cycles*, v. 30, no. 2, p. 211-218.

657 Weber, M. E., Clark, P. U., Kuhn, G., Timmermann, A., Sprenk, D., Gladstone, R., Zhang, X.,
658 Lohmann, G., Menviel, L., Chikamoto, M. O., Friedrich, T., and Ohlwein, C., 2014,
659 Millennial-scale variability in Antarctic ice-sheet discharge during the last deglaciation:
660 *Nature*, v. 510, no. 7503, p. 134-138.

661 Wessel, P. a. S., W.H., , 1998, New, improved version of Generic Mapping Tools released.: *Eos*,
662 *Transactions American Geophysical Union*, v. 79, no. 47, p. 579-579.

663 Willey, J. D., Kieber, R.J., Eyman, M.S., Avery Jr., G.B., 2, 2000, Rainwater dissolved organic
664 carbon: concentrations and global flux. : *Global Biogeochemical Cycles*, v. 14, p. 139–
665 148.

666 Winter, K., Woodward, J., Dunning, S. A., Turney, C. S., Fogwill, C. J., Hein, A. S., Golledge,
667 N. R., Bingham, R. G., Marrero, S. M., and Sugden, D. E., 2016a, Assessing the
668 continuity of the blue ice climate record at Patriot Hills, Horseshoe Valley, West
669 Antarctica: *Geophysical Research Letters*, v. 43, no. 5, p. 2019-2026.

670 Winter, K., Woodward, J., Dunning, S. A., Turney, C. S. M., Fogwill, C. J., Hein, A. S., Golledge,
671 N. R., Bingham, R. G., Marrero, S. M., Sugden, D. E., and Ross, N., 2016b, Assessing the

672 continuity of the blue ice climate record at Patriot Hills, Horseshoe Valley, West
673 Antarctica: *Geophys. Res. Lett.*, v. 10.1002/2015GL066476.

674 Wolff, E., Fischer, H., Fundel, F., Ruth, U., Twarloh, B., Littot, G., Mulvaney, R., Rothlisberger,
675 R. d. A., M., , Boutron, C., Hansson, M., Jonsell, U., Hutterli, M., Lambert, F., Kaufmann,
676 P., Stauffer, B., Stocker, T., Steffensen, J., Bigler, M., Siggaard-Andersen, M., Udisti, R.,
677 Becagli, S., Castellano, E., Severi, M., Wagenbach, D., Barbante, C., Gabrielli, P., and
678 Gaspari, V., 2006a, Southern Ocean sea-ice extent, productivity and iron flux over the
679 past eight glacial cycles. : *Nature*, v. 440, p. 491-496.

680 Wolff, E. W., Fischer, H., Fundel, F., Ruth, U., Twarloh, B., Littot, G. C., Mulvaney, R.,
681 R thlisberger, R., de Angelis, M., Boutron, C. F., Hansson, M., Jonsell, U., Hutterli, M.
682 A., Lambert, F., Kaufmann, P., Stauffer, B., Stocker, T. F., Steffensen, J. P., Bigler, M.,
683 Siggaard-Andersen, M. L., Udisti, R., Becagli, S., Castellano, E., Severi, M., Wagenbach,
684 D., Barbante, C., Gabrielli, P., and Gaspari, V., 2006b, Southern Ocean sea-ice extent,
685 productivity and iron flux over the past eight glacial cycles: *Nature*, v. 440, no. 7083, p.
686 491-496.
687

688

689

690

691

692

693

694

695

696

697

698